Journal of
Marine Science and Engineering

MDPI

Article

Scattering Study of a Composite Breakwater Placed in Front of an Impermeable Back Wall under the Action of Water Waves

Jiaxiu Cao [1], Chao Wang [1] and Zeping Wang [1,2,*]

[1] College of Shipbuilding Engineering, Harbin Engineering University, Harbin 150001, China
[2] Qingdao Innovation and Development Center, Harbin Engineering University, Qingdao 266000, China
* Correspondence: zepwang@hrbeu.edu.cn

Abstract: Based on the assumption of linear potential flow theory, the scattering problem of a composite breakwater placed in front of an impermeable back wall is theoretically investigated. The velocity potential in each subregion is found using the eigenfunction expansion method. The boundary conditions of the porous region are treated using Darcy's law. The semi-analytical solution of a composite breakwater placed in front of an impermeable back wall is then obtained based on the matching conditions of the boundaries of the different regions. The effects of different parameters on the wave loads and wave amplitudes are investigated. In addition, to better understand the performance of the composite breakwater, the scattering problem of the composite breakwater without considering an impermeable back wall is also investigated. The correctness of this theoretical model is verified by comparing the results with previous work. Based on the results of hydrodynamic calculations and analysis of various aspects of a composite breakwater placed in front of an impermeable back wall, the study of the effect of a composite breakwater placed in front of an impermeable back wall allows us to propose a long-term and cost-effective solution for the protection of various marine facilities from wave attacks.

Keywords: composite breakwater; porosity; wave scattering; hydrodynamic force

Citation: Cao, J.; Wang, C.; Wang, Z. Scattering Study of a Composite Breakwater Placed in Front of an Impermeable Back Wall under the Action of Water Waves. *J. Mar. Sci. Eng.* **2023**, *11*, 1878. https://doi.org/10.3390/jmse11101878

Academic Editor: Luca Cavallaro

Received: 16 August 2023
Revised: 18 September 2023
Accepted: 26 September 2023
Published: 27 September 2023

1. Introduction

Studies have shown that porous breakwaters are effective at reducing wave forces acting on structures and reducing wave run-up. Additionally, porous breakwaters can prevent wave damage to coastal and offshore infrastructure. As sea levels rise due to global warming, the use of porous breakwaters in coastal engineering for harbor and coastline protection is increasing. Porous structures are very flexible and can be reused, which helps to reduce costs. Due to the large number of porous structures used in the ocean, the research on the use of porous structures in waves is increasing. Meanwhile, the use of composite porous structures is increasing. The study of water waves and porous structures can provide theoretical support for the design of marine structures, such as offshore fish cages and tension-leg platforms, so it is important to study the interaction between water waves and porous structures.

When studying porous breakwaters, it has been found that increasing the number of layers of the porous plate can provide better wave dissipation. To investigate whether increasing the number of layers of porous cylinders can also provide better wave attenuation effects, a new type of porous structure—a composite porous structure—is proposed based on practical engineering. The purpose is to design an efficient porous breakwater. It is used to study the scattering problem of composite porous structures placed in front of impermeable walls. Due to the advantages of non-directional hydrodynamic effects and its frequent use on coastal and offshore structures, the composite porous structure is designed with a cylindrical shape. The structure and research methodology used for the model proposed in this paper share similarities with existing studies. Therefore, they can be adopted from existing studies. Meanwhile, there are many studies on cylindrical structures that can provide a basis and foundation for the research performed in this paper.

In recent decades, many researchers have studied wave scattering orginating from various types of porous structure, including horizontal porous plates (Liu et al. [1]; Athul Krishna et al. [2]), caisson breakwaters (Lee and Shin [3]; Zhao et al. 2020 [4]), and partially perforated breakwaters (Li et al. 2005 [5]; Suh et al. 2006 [6]). Researchers have made some important advances in water wave scattering originating from porous structures. Jarlan [7] proposed the concept of a perforated-wall caisson breakwater, and this type of breakwater is now named after him. Jarlan-type breakwaters consist of a perforated front wall and a vertical impermeable back wall. The first analytical model was based on acoustic theory (Jarlan [8]). Scholars have proposed a number of different designs of perforated breakwaters based on the Jarlan-type breakwater, such as those of Isaacson et al. [9] and Garrido and Medina [10]. Garrido used a new semi-empirical model to study the coefficients of reflection for the single-hole and double-hole models of Jarlan-type breakwaters. Yang et al. [11] studied the interaction of a linear water wave impinging on a vertical thin, porous breakwater at a constant depth. A case was studied in which a semi-submerged fixed rectangular obstacle was placed in front of it. Williams et al. [12] proposed a simplified analytical solution for modeling the interaction between linear waves and absorbing caisson breakwaters with one or two perforated or slotted front surfaces. Li et al. [13] investigated the reflection of oblique incident waves from breakwaters consisting of a double-layered perforated wall and an impermeable back wall. Liu and Li [14], Liu et al. [15], Liu et al. [16], and Mohapatra and Sahoo [17] also conducted studies on other models of impermeable and permeable types. In addition, porous structures placed on a two-layer fluid/uneven seabed in front of an impermeable back wall have also been studied (Behera and Sahoo [18]; Chang and Tsai [19]). The studies described above all employed single porous structures. As research progressed, Tsai et al. [20] investigated the placement of multiple porous structures in front of an impermeable back wall.

At the same time, the interaction of water waves with compound cylinders has a certain stability that has also attracted the attention of several researchers, who conducted an in-depth study of the key properties of concentric structures. The key properties include the permeability coefficient and the inner and outer radius ratios, as these are the key factors influencing the protective effect of the outer cylinder on the inner cylinder. More recently, Zhai et al. [21] studied the diffraction problem of solitary waves interacting with two thin concentric asymmetric porous arc-wall assembled structures using the eigenfunction expansion method. In 2021, Zhai et al. [22] also used the eigenfunction expansion method to conduct a theoretical study on the interaction between Airy waves and a perforated concentric double-arc porous wall on a bottom-mounted surface. Williams and Li [23] used the eigenfunction expansion method to theoretically study the enclosure problem of a rigid vertical cylinder mounted on a storage tank. Sankarbabu et al. [24] investigated the diffraction problem of an array of porous cylinders under the action of linear waves using the eigenfunction expansion method. The model described in this paper includes a porous outer cylinder and a rigid inner cylinder. Liu et al. [25] investigated the diffraction problem of a cylindrical structure with a porous surface under the action of waves using the semi-analytical scaled-boundary finite element method (SBFEM). The coaxial cylindrical structure consisted of a rigid inner cylinder and two porous outer cylinders. Ning et al. [26] investigated the diffraction problem of a composite truncated cylinder at a finite water depth using the variable separation method and the eigenfunction expansion technique. The truncated top cylinder included a porous upper sidewall and an inner cylinder. Park and Jeong [27] investigated the diffraction problem of an array of porous cylindrical structures using the eigenfunction expansion method. The porous cylinder consisted of a rigid inner cylinder and a porous outer cylinder. Liu et al. [28] proposed an analytical method for the study of coaxial porous cylindrical systems with arbitrary smooth cross-sections. The multilayer coaxial porous cylindrical system consisted of a rigid inner cylinder and a single-layer porous outer cylinder. Sarkar and Bora [29] studied a series of linear water waves incident on a bottom-mounted porous composite cylinder composed of two coaxial cylinders using the eigenfunction expansion method. The upper cylinder is hollow with thin, porous sidewalls, while the radius of the lower cylinder is greater than that of the upper cylinder, and the lower cylinder is rigid.

The studies described above show that the structure placed in front of the impermeable back wall consists of a single layer, and no research has been carried out on coaxial composite porous structures placed in front of impermeable back walls. Meanwhile, reading the extensive literature reveals that the model described in this paper has not been studied. It is a new, more complex structure than existing models. The model described in this paper contains an outer cylinder and an inner cylinder, with holes in the walls of both the inner and outer cylinders. Based on existing research, a new composite breakwater model is proposed in which the porous structure and the composite cylinder are combined. As can be seen from Figure 1b, the composite breakwater is a concentric and symmetric composite cylinder with porosities in both the outer cylinder wall ($z \geq -h_2$) and inner cylinder wall ($-h_2 \leq z \leq -h_1$), the lower wall of the outer cylinder ($-d \leq z \leq -h_2$) is not porous, and the remaining part of the cylinder wall ($z \geq -h_2$) is porous, the upper wall ($z \geq -h_1$) and the lower wall ($-d \leq z \leq -h_2$) of the inner cylinder are not porous, and the remaining part of the cylinder wall ($-h_2 \leq z \leq -h_1$) is porous. The main work in this paper consists of a theoretical study of the scattering problem of a composite breakwater placed in front of an impermeable back wall at a finite water depth. Under the assumption of the linear theory of potential flow, the eigenfunction expansion method is used to study this. It is also compared with the results of existing research in order to verify the accuracy of the model proposed in this paper. To understand the performance of an composite breakwater placed in front of an impermeable back wall, the force and moment acting on it are calculated and analyzed using various structural parameters. Meanwhile, to understand the hydrodynamic performance of the composite breakwater, studies are conducted on the effect of the porosity G, the radius ratio a/b, and the ratio h_2/h_1 on the composite breakwater. The composite breakwater is also studied using the same method. The results of this paper can serve as a valuable reference for the subsequent predesign and study of breakwater systems in practical engineering applications.

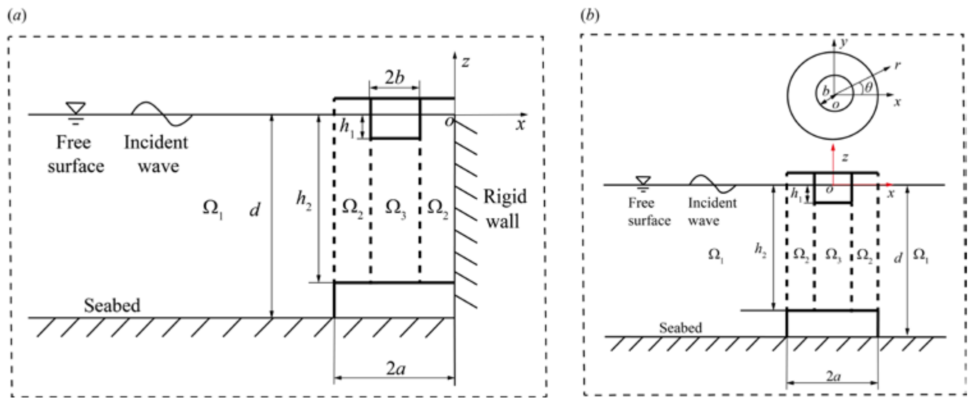

Figure 1. Schematic diagram of the structures. (**a**) A composite breakwater placed in front of an impermeable back wall (a 2D problem). (**b**) A composite breakwater (a 3D problem).

The structure of this paper can be described as follows: A mathematical description of the problem is given in Section 2. The analytical solution of the velocity potential is given in Section 3, where the wave force and wave elevation are calculated on the basis of the velocity potential. The results of the model validation and parametric study are given in Section 4, and the conclusions are given in Section 5.

2. Mathematical Formulation

2.1. A Composite Breakwater Placed in front of an Impermeable Back Wall

A geometric schematic of the two-dimensional problem is shown in Figure 1a. This paper uses the small-amplitude water wave theory to analyze the scattering problem of a composite breakwater placed on a vertically impermeable back wall under finite water depth conditions in a Cartesian coordinate system. Here, the parameter d denotes the constant water depth. The parameter a denotes the radius of the outer cylinder, and the parameter b denotes the radius of the inner cylinder. The parameter h_1 denotes the height of the impermeable part of the upper cylinder and of the inner cylinder, and h_2 denotes the height of the permeable part of the outer cylinder. The origin of the Cartesian coordinate system $(x,\ z)$ is located at the still-water level. The $z-$axis runs vertically upward along the back wall of the solid, and the $x-$axis points out of the fluid domain. The composite breakwater placed in front of an impermeable back wall is affected by normally incident regular waves with a height of H ($H = 2A$, where A denotes amplitude) and an angular wave frequency of ω. The whole fluid domain is divided into three regions: (1) region I: $x \leq -2a, 0 \leq z \leq -d$; (2) region II: $b-a \leq x \leq 0,\ -2a \leq x \leq -b-a,\ -h_2 \leq z \leq 0$; (3) region III: $b-a \leq x \leq -a,\ -h_2 \leq z \leq -h_1$. In this study, the thickness of both the outer and inner cylinders is assumed to be zero. This is because their thicknesses are very small compared to the incident wavelength. The fluid considered in this paper is homogeneous, inviscid and incompressible. Additionally, the motion is non-rotational. The velocity potential $\Phi(x,z,t)$ can be expressed as

$$\Phi(x,\ z,\ t) = \mathrm{Re}[\phi(x,\ z)e^{-\mathrm{i}\omega t}], \tag{1}$$

where Re denotes the real part, $\mathrm{i} = \sqrt{-1}$ the imaginary unit, ω the angular wave frequency of the incoming waves, t the time, and ϕ the spatial velocity potential.

Thus, in different regions, the spatial velocity potential $\phi_j, j = 1,\ 2, 3$ in each fluid region satisfies Laplace's equation:

$$\frac{\partial^2 \phi_j(x,z)}{\partial x^2} + \frac{\partial^2 \phi_j(x,z)}{\partial z^2} = 0,\ j = 1,\ 2,\ 3, \tag{2}$$

where j represents the variables concerning the region j.

It is also necessary for the spatial velocity potential $\phi_j, j = 1,\ 2, 3$ to satisfy the boundary conditions in the different regions $I,\ II,\ III$, respectively.

The boundary conditions at the free surface and on the seabed can be written as follows:

$$\frac{\partial \phi_j}{\partial z} = \frac{\omega^2}{g}\phi_j,\ z = 0,\ j = 1,\ 2, \tag{3}$$

$$\frac{\partial \phi_1}{\partial z} = 0,\ z = -d, \tag{4}$$

$$\frac{\partial \phi_2}{\partial z} = 0,\ z = -h_2, \tag{5}$$

$$\frac{\partial \phi_3}{\partial z} = 0,\ z = -h_1, \tag{6}$$

$$\frac{\partial \phi_3}{\partial z} = 0,\ z = -h_2, \tag{7}$$

$$\frac{\partial \phi_2}{\partial x} = 0,\ x = 0. \tag{8}$$

The boundary conditions on the impermeable surface of the cylinder can be expressed as follows:

$$\frac{\partial \phi_1}{\partial x} = 0,\ x = -2a,\ -d \le z \le -h_2, \tag{9}$$

$$\frac{\partial \phi_2}{\partial x} = 0,\ x = -a - b,\ -h_1 \le z \le 0. \tag{10}$$

The boundary conditions on the porous cylinder wall can be expressed as follows (Williams and Li [12]; Williams et al. [30]):

$$\frac{\partial \phi_2}{\partial x} = \mathrm{i}G(\phi_2 - \phi_1),\ x = -2a,\ -h_2 \le z \le 0, \tag{11}$$

$$\frac{\partial \phi_2}{\partial x} = \epsilon \frac{\partial \phi_3}{\partial x},\ x = -a - b,\ -h_2 \le z \le -h_1, \tag{12}$$

$$\phi_2 = (m - \mathrm{i}f)\phi_3,\ x = -a - b,\ -h_2 \le z \le -h_1, \tag{13}$$

where G denotes the porous effect parameter, ϵ the porosity of the permeable material, m the inertial coefficient, and f the linearized friction coefficient. The study by Williams et al. [30] gives a detailed explanation of the porous effect parameter $G = \rho\omega\gamma/(\mu k)$, where μ denotes the constant coefficient of dynamic viscosity, γ a material constant having the dimension of length, ρ the fluid density, and k the incident wavenumber. In this article, when $\epsilon = 1$, $m = 1$, and $f = 0$, they have the same range as that described in Dalrymple et al. [31] and Behera and Sahoo [18]. Barman and Bora [32] carried out a detailed study of the resistance effect of porous materials on flow and derived the relevant equations for the porous parameters.

Along the interfaces between region I and region II, the spatial velocity potential should satisfy the following matching condition:

$$\frac{\partial \phi_1}{\partial x} = \frac{\partial \phi_2}{\partial x},\ x = -2a,\ -h_2 \le z \le 0 \tag{14}$$

2.2. A Composite Breakwater

To fully understand the performance of the composite breakwater, especially without considering the presence of an impermeable back wall, relevant research is conducted. In this paper, we consider a three-dimensional problem in a cylindrical coordinate system (r, θ, z), with the origin located on the mean free surface $z = 0$ and with the $z-$axis up. This paper also considers a train of the small-amplitude wave propagating from $-\infty$ towards the composite breakwater. The scattering problem for a composite breakwater is considered, as shown in Figure 1b. The fluid domain is divided into the following three regions: (1) region I: $r \ge a, -d \le z \le 0$; (2) region II: $b \le r \le a, -h_2 \le z \le 0$; (3) region III: $0 \le r \le b, -h_2 \le z \le -h_1$. The fluid is inviscid and incompressible. The motion is non-rotational. According to the linear potential flow theory, the fluid flow can be described by introducing the velocity potential as follows:

$$\psi(r,\ \theta,\ z,\ t) = \mathrm{Re}[\varphi(r,\ \theta,\ z)e^{-\mathrm{i}\omega t}], \tag{15}$$

where Re denotes the real part of the argument, $\mathrm{i} = \sqrt{-1}$, ω the angular wave frequency of the incoming waves, t the time, and φ the spatial velocity potential.

In the flow region, each potential needs to satisfy Laplace's equation:

$$\nabla^2 \varphi_j = 0,\ j = 1,\ 2,\ 3, \tag{16}$$

where $\varphi_j,\ j = 1,\ 2,\ 3$ denotes the velocity potential in each region.

The boundary conditions at the free surface and the seabed are as follows:

$$\frac{\partial \varphi_j}{\partial z} - \frac{\omega^2}{g}\varphi_j = 0,\ z = 0,\ j = 1,\ 2, \tag{17}$$

$$\frac{\partial \varphi_1}{\partial z} = 0,\ z = -d, \tag{18}$$

$$\frac{\partial \varphi_2}{\partial z} = 0,\ z = -h_2, \tag{19}$$

$$\frac{\partial \varphi_3}{\partial z} = 0,\ z = -h_1, \tag{20}$$

$$\frac{\partial \varphi_3}{\partial z} = 0,\ z = -h_2. \tag{21}$$

The boundary conditions on the surface of the rigid cylinder are as follows:

$$\frac{\partial \varphi_1}{\partial r} = 0,\ r = a,\ -d \le z \le -h_2, \tag{22}$$

$$\frac{\partial \varphi_2}{\partial r} = 0,\ r = b,\ -h_1 \le z \le 0. \tag{23}$$

The boundary conditions on the porous cylinder wall are as follows (Williams and Li [12]; Williams et al. [30]):

$$\frac{\partial \varphi_2}{\partial r} = \mathrm{i}G(\varphi_2 - \varphi_1),\ r = a,\ -h_2 \le z \le 0, \tag{24}$$

$$\frac{\partial \varphi_2}{\partial r} = \epsilon \frac{\partial \varphi_3}{\partial r},\ r = b,\ \ -h_2 \le z \le -h_1, \tag{25}$$

$$\varphi_2 = (m - \mathrm{i}f)\varphi_3,\ r = b,\ -h_2 \le z \le -h_1, \tag{26}$$

where G denotes the porous effect parameter, ϵ the porosity of the permeable material, m the inertial coefficient, and f the linearized friction coefficient. These parameters take the same values as those described above.

Along the interfaces between region I and region II, the spatial velocity potential should satisfy the following matching condition:

$$\frac{\partial \varphi_1}{\partial r} = \frac{\partial \varphi_2}{\partial r},\ r = a,\ -h_2 \le z \le 0. \tag{27}$$

At infinity, the velocity potential in the exterior region must satisfy the Sommerfeld radiation condition, that is:

$$\lim_{r\to\infty}\sqrt{r}\left[\frac{\partial(\varphi_1 - \varphi_I)}{\partial r} - \mathrm{i}k(\varphi_1 - \varphi_I)\right] = 0, \tag{28}$$

where φ_I is the incident velocity potential.

3. Analytical Solution of Velocity Potential

3.1. A Composite Breakwater Placed in front of an Impermeable Back Wall

The velocity potential ϕ_1 satisfies Equations (2)–(4), and using the separation of variables method, it can be found that

$$\phi_1(x,\ z) = -\frac{\mathrm{i}gH}{2\omega}\left[\mathrm{e}^{\mathrm{i}k_0^{(1)}(x+2a)}Z_0^{(1)}(z) + \sum_{m=0}^{\infty} A_m \mathrm{e}^{k_m^{(1)}(x+2a)}Z_m^{(1)}(z)\right], \tag{29}$$

where A_m $(m = 0, 1, 2, \ldots)$ are the unknown expansion coefficients. The depth-dependent functions $Z_m^{(1)}(z)$ $(m = 0, 1, 2, \ldots)$ can be defined as

$$Z_m^{(1)}(z) = \begin{cases} \frac{\cosh k_0^{(1)}(z+d)}{\cosh k_0^{(1)} d}, & m = 0 \\ \frac{\cos k_m^{(1)}(z+d)}{\cos k_m^{(1)} d}, & m \geq 1 \end{cases}. \tag{30}$$

The wave numbers $k_0^{(1)}$ and $k_m^{(1)}$ $(m = 1, 2, \ldots)$ are the positive real roots of the following dispersion relations (as shown in the study by Losada et al. [33]):

$$\omega^2 = gk_0^{(1)} \tanh k_0^{(1)} d = -gk_m^{(1)} \tan k_m^{(1)} d,\ m = 1, 2, \ldots. \tag{31}$$

The velocity potential ϕ_2 and ϕ_3, satisfying Equations (2),(3) and (5)–(8), can be obtained as follows:

$$\phi_2(x, z) = -\frac{\mathrm{i}gH}{2\omega} \sum_{q=0}^{\infty} B_q Z_q^{(2)}(z) (\mathrm{e}^{k_q^{(2)} x} + \mathrm{e}^{-k_q^{(2)} x}), \tag{32}$$

$$\phi_3(x, z) = -\frac{\mathrm{i}gH}{2\omega} \sum_{n=0}^{\infty} (C_n \mathrm{e}^{\kappa_n x} + D_n \mathrm{e}^{-\kappa_n x}) \cos \frac{n\pi(z + h_2)}{h_2 - h_1}, \tag{33}$$

where B_q $(q = 0, 1, 2, \ldots)$, C_n $(n = 0, 1, 2, \ldots)$, and D_n $(n = 0, 1, 2, \ldots)$ are the unknown expansion coefficients.

The depth-dependent functions $Z_q^{(2)}(z)$ are given by the following forms:

$$Z_q^{(2)}(z) = \begin{cases} \frac{\cosh k_0^{(2)}(z+h_2)}{\cosh k_0^{(2)} h_2}, & q = 0 \\ \frac{\cos k_q^{(2)}(z+h_2)}{\cos k_q^{(2)} h_2}, & q \geq 1 \end{cases}. \tag{34}$$

The wave numbers $k_0^{(2)}$ and $k_q^{(2)}$ $(q = 1, 2, \ldots)$ are the positive real roots of the following dispersion relations (as shown in the study by Losada et al. [33]):

$$\omega^2 = gk_0^{(2)} \tanh k_0^{(2)} h_2 = -gk_q^{(2)} \tan k_q^{(2)} h_2,\ q = 1, 2, \ldots. \tag{35}$$

In this paper, matched porous boundary conditions are used to solve for the unknown complex coefficients A_m, B_q, C_n, and D_n. A system of linear algebraic equations is generated to solve these unknown complex coefficients via the truncation of an infinite series over a particular finite term for the unknown coefficients A_m, B_q, C_n, and D_n. In this paper, the standard matrix technique is used to solve this problem. After the unknown expansion coefficients A_m, B_q, C_n, and D_n have been derived, the force and moment can be obtained by integrating over the velocity potential.

The horizontal wave force F_x and the moment M_x are given as follows:

$$F_{x1} = \mathrm{i}\rho\omega \int_{-h_2}^{0} (\phi_1 - \phi_2) dz,\ x = -2a, \tag{36}$$

$$M_{x1} = \mathrm{i}\rho\omega \int_{-h_2}^{0} (\phi_1 - \phi_2)(d + z) dz,\ x = -2a \tag{37}$$

$$F_{x2} = \mathrm{i}\rho\omega \int_{-h_2}^{-h_1} (\phi_2 - \phi_3) dz,\ x = -2b, \tag{38}$$

$$M_{x2} = \mathrm{i}\rho\omega \int_{-h_2}^{-h_1} (\phi_2 - \phi_3)(d + z) dz,\ x = -2b, \tag{39}$$

where F_{x1} and M_{x1} denote the wave force and moment acting on the outer cylinder, respectively. F_{x2} and M_{x2} denote the wave force and moment acting on the inner cylinder, respectively.

The surface elevation $\eta(x)$ of water waves can be obtained as follows:

$$\eta(x) = -\frac{\mathrm{i}\omega}{g}\varphi(x,\, z),\; z = 0. \tag{40}$$

3.2. A Composite Breakwater

The separation of variables method is applied to each region to obtain an expression for the associated velocity potential. The velocity potential φ_1 for the region I takes the following form:

$$\varphi_1(r,\,\theta,\,z) = -\frac{\mathrm{i}gH}{2\omega}\sum_{m=0}^{\infty}\left[S_0(z)K_0(r)\mathrm{i}^m + \sum_{q=0}^{\infty} A_{mq}T_{mq}^{(1)}(r)Z_q^{(1)}(z)\right]\mathrm{e}^{\mathrm{i}m\theta}, \tag{41}$$

where A_{mq} $(q = 0,\, 1,\, 2,\, 3, \ldots)$ are the unknown expansion coefficients.

The wave number $\kappa_0^{(1)}$ and $\kappa_q^{(1)}$ $(q = 1,\, 2,\, 3, \ldots)$ can be derived using the following dispersion relations (as shown in the study by Losada et al. [33]):

$$\omega^2 = g\kappa_0^{(1)}\tanh\kappa_0^{(1)}d = -g\kappa_q^{(1)}\tan\kappa_q^{(1)}d,\; q = 1,\, 2,\, 3, \ldots. \tag{42}$$

The radial eigenfunctions $T_{mq}^{(1)}(r)$ are as follows:

$$T_{mq}^{(1)}(r) = \begin{cases} \dfrac{H_m^{(1)}(\kappa_0^{(1)}r)}{H'^{(1)}_m(\kappa_0^{(1)}a)}, & q = 0 \\ \dfrac{K_m(\kappa_q^{(1)}r)}{K'_m(\kappa_q^{(1)}a)}, & q \geq 1 \end{cases}, \tag{43}$$

where $H_m^{(1)}$ denotes the Hankel function of the first kind, K_m the modified Bessel function of the second kind, $H'^{(1)}_m$ the first derivatives of the Hankel function, and K'_m the first derivatives of the modified Bessel function.

The vertical eigenfunction $Z_q^{(1)}(z)$ can be obtained as follows:

$$Z_q^{(1)}(z) = \begin{cases} \dfrac{\sqrt{2}\cosh\kappa_0^{(1)}(z+d)}{\sqrt{1+\frac{\sinh 2\kappa_0^{(1)}d}{2\kappa_0^{(1)}d}}}, & q = 0 \\ \dfrac{\sqrt{2}\cos\kappa_q^{(1)}(z+d)}{\sqrt{1+\frac{\sin 2\kappa_q^{(1)}d}{2\kappa_q^{(1)}d}}}, & q \geq 1 \end{cases}. \tag{44}$$

$S_0(z)$ and $K_0(r)$ can be obtained as

$$S_0(z) = \frac{\cosh\kappa_0^{(1)}(z+d)}{\cosh\kappa_0^{(1)}d}, \tag{45}$$

$$K_0(r) = \frac{J_m(\kappa_0^{(1)}r)H'_m(\kappa_0^{(1)}a) - J'_m(\kappa_0^{(1)}a)H_m^{(1)}(\kappa_0^{(1)}r)}{H'_m(\kappa_0^{(1)}a)}, \tag{46}$$

where J_m denotes the Bessel function of the first kind, J'_m denotes the first derivative of the Bessel function.

The velocity potential φ_2 is obtained as follows:

$$\varphi_2(r,\ \theta,\ z) = -\frac{\mathrm{i}gH}{2\omega}\sum_{m=-\infty}^{\infty}\sum_{n=0}^{\infty} B_{mn} T_{mn}^{(2)}(r) Z_n^{(2)}(z) \mathrm{e}^{\mathrm{i}m\theta}, \tag{47}$$

where B_{mn} $(n = 0,\ 1,\ 2,\ 3, \ldots)$ are the unknown expansion coefficients.

The wave number $\kappa_0^{(2)}$ and $\kappa_n^{(2)}$ $(n = 1,\ 2,\ 3, \ldots)$ can be derived using the following dispersion relations (as in the study by Losada et al. [33]):

$$\omega^2 = g\kappa_0^{(2)} \tanh\kappa_0^{(2)} h_2 = -g\kappa_n^{(2)} \tan \kappa_n^{(2)} h_2,\ n = 1,\ 2,\ 3, \ldots. \tag{48}$$

The radial eigenfunctions $T_{mn}^{(2)}(r)$ are as follows:

$$T_{mn}^{(2)}(r) = \begin{cases} \frac{H_m^{(1)}(\kappa_0^{(2)} r)}{H'^{(1)}_m(\kappa_0^{(2)} a)}, & n = 0 \\ \frac{K_m(\kappa_n^{(2)} r)}{K'_m(\kappa_n^{(2)} a)}, & n \geq 1 \end{cases}. \tag{49}$$

The vertical eigenfunction $Z_n^{(2)}(z)$ can be obtained as

$$Z_n^{(2)}(z) = \begin{cases} \frac{\sqrt{2}\cosh \kappa_0^{(2)}(z+h_2)}{\sqrt{1+\frac{\sinh 2\kappa_0^{(2)} h_2}{2\kappa_0^{(2)} h_2}}}, & n = 0 \\ \frac{\sqrt{2}\cos \kappa_n^{(2)}(z+h_2)}{\sqrt{1+\frac{\sin 2\kappa_n^{(2)} h_2}{2\kappa_n^{(2)} h_2}}}, & n \geq 1 \end{cases}. \tag{50}$$

The velocity potential φ_3 is obtained as follows:

$$\varphi_3(r,\theta,z) = -\frac{\mathrm{i}gH}{2\omega}\sum_{m=0}^{\infty}\sum_{l=0}^{\infty} C_{ml} V_l^m(r) U_l(z) e^{-\mathrm{i}m\theta}, \tag{51}$$

where C_{ml} $(l = 0,\ 1,\ 2,\ 3, \ldots)$ are the unknown expansion coefficients.

$V_l^m(r)$ and $U_l(z)$ can be obtained as

$$V_l^m(r) = \begin{cases} \left(\frac{r}{a}\right)^{|m|}, & l = 0 \\ \frac{I_m\left(\frac{l\pi r}{h_2-h_1}\right)}{I_m\left(\frac{l\pi b}{h_2-h_1}\right)}, & l \geq 1 \end{cases}, \tag{52}$$

$$U_l(z) = \begin{cases} \frac{1}{2}, & l = 0 \\ \cos \frac{l\pi(z+h_2)}{h_2-h_1}, & l \geq 1 \end{cases}, \tag{53}$$

By solving for the unknown coefficients using the same method as described above, the horizontal wave force f_x can be determined as follows:

$$f_{x1} = \mathrm{i}\rho\omega\left(\int_0^{2\pi}\int_{-h_2}^{0} \varphi_1 \cos(\pi-\theta) d\theta dz - \int_0^{2\pi}\int_{-h_2}^{0} \varphi_2 \cos(\pi-\theta) d\theta dz\right),\ x = a, \tag{54}$$

$$f_{x2} = \mathrm{i}\rho\omega\left(\int_0^{2\pi}\int_{-h_2}^{-h_1} \varphi_2 \cos(\pi-\theta) d\theta dz - \int_0^{2\pi}\int_{-h_2}^{-h_1} \varphi_3 \cos(\pi-\theta) d\theta dz\right),\ x = b, \tag{55}$$

where f_{x1} and f_{x2} denote the wave force on the outer cylinder and the inner cylinder, respectively.

The wave amplitude $\zeta(x)$ of water waves can be obtained as follows:

$$\zeta(x) = -\frac{i\omega}{g}\varphi(r,\ \theta,\ z),\ z = 0. \tag{56}$$

4. Numerical Results and Discussion

4.1. Validation

The reduced model proposed in this paper is equivalent to the models used in previous studies. The computational results of the reduced model are compared with those of existing models in order to verify the correctness of the results reported in this paper.

Wu et al. [34] investigated the reflection of water waves by a vertical wall with a porous structure. A comparison of the reflection coefficient K_R obtained using our model with that obtained by Wu et al. [34] is shown in Figure 2a. The calculated parameters are $G = 0$, $h/L = 0.25$ and $b/h = 0.2$, where G denotes the porous effect parameter, h the water depth, L the wavelength, and b the submerged depth of the structure. It can be observed that the results reported in this paper are consistent with the results of Wu et al. [34].

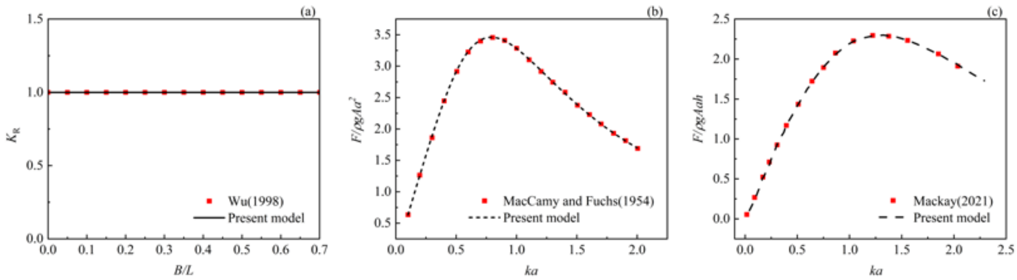

Figure 2. Comparison of the results obtained in the present work with those previously reported by (**a**) Wu et al. [34], (**b**) MacCamy and Fuchs [35], and (**c**) Mackay et al. [36].

MacCamy and Fuchs [35] applied the theory to the calculation of wave forces on rigid cylindrical surfaces. Figure 2b shows the calculation results obtained when using the reduced model in comparison with the data reported by MacCamy and Fuchs [35]. The calculated parameters are $a = d$, $\beta = 2\pi$ and $G = 0$, where a denotes the radius, d the water depth, β the wave incidence angle, and G the porous effect parameter. The comparison results are shown in Figure 2b, and the results are in good agreement.

Mackay et al. [36] calculated the hydrodynamics of the porous outer cylinder. Figure 2c shows the result of a comparison of the present model with surface porosity and that of Mackay et al. [36]. The seabed porosity parameter was set to $G_1 = 0$, the cylinder wall surface porosity $G = 0.1$, and $a/d = 1/4$, where a denotes the radius and d the draft of the outer cylinder from the free surface. The comparison results are shown in Figure 2c, and the results are in good agreement.

In summary, the correctness of the results derived using our model formulation proves the validity the model.

4.2. Results and Discussion

To study the hydrodynamic performance of the composite breakwater, a computer program was written to implement the above analytical solution. First, the convergence of the method in which the expansion coefficients are calculated using the truncation numbers M and N is investigated. The results of the horizontal wave forces f_{x1} acting on the outer cylinder of the composite breakwater for different values of M and N are shown in Table 1. Here, the basic parameters are: $\beta = 0^\circ, a/b = 4,\ d/h_1 = 10,\ d/h_2 = 5/4$ and $G = 1$. It can be clearly seen from the table that the truncation number M $= 15$ should be selected. For the other model (the composite breakwater placed in front of an impermeable back wall) in this paper, the same method is used to obtain M $= 25$.

Table 1. Convergence of forces f_{x1} for different values of M and N.

Truncation Numbers	Forces f_{x1}					
	ka = 0.1	ka = 0.2	ka = 0.3	ka = 0.4	ka = 0.5	ka = 0.6
5	0.227671	0.167398	0.567639	1.170995	1.10001	1.006249
10	0.639971	0.188992	0.407563	0.671492	0.884464	1.104123
15	0.306343	0.375348	0.420938	0.357601	0.161683	0.498337
20	0.306343	0.375348	0.420938	0.357601	0.161683	0.498337
25	0.306343	0.375348	0.420938	0.357601	0.161683	0.498337
30	0.306343	0.375348	0.420938	0.357601	0.161683	0.498337

In order to validate the present solution, a detailed parametric study is conducted to investigate the effects of the porosity G, radius ratio a/b, and the ratio h_2/h_1 on the wave force and moment acting on the composite breakwater placed in front of an impermeable back wall. In all subsequent calculations, the wave force and moment of the model (the composite breakwater placed in front of an impermeable back wall) are non-dimensionalized by $\rho g H d$ and $\rho g H d^2$, respectively. The wave force of the model (the composite breakwater) is non-dimensionalized by $\rho g H \pi a^2$, and the magnitude of free-surface elevation is non-dimensionalized by $H/2$. Additionally, we make the wavenumber dimensionless (the wavenumber is multiplied by the radius of the outer cylinder) in order to obtain the dimensionless wavenumber ka. In the following calculations, the angles of incidence are all $\beta = 0^\circ$.

4.2.1. A Composite Breakwater Placed in front of an Impermeable Back Wall

In Figure 3, the dimensionless wave force $|F_{x1}/\rho g H d|$ and the dimensionless moment $\left|M_{x1}/\rho g H d^2\right|$ for a composite breakwater placed in front of an impermeable back wall are plotted against the dimensionless wavenumber ka for various values of G corresponding to $a/b = 3$, $h_1/d = 1/5$, $h_2/d = 4/5$ and $\beta = 0^\circ$. For $G = 0.5$, the dimensionless wave force and moment distributions of the outer cylinder follow the same trend as that observed when $G = 1.0$ and 1.5. It can be seen that the maximum force on the outer cylinder occurs around the dimensionless wavenumber of 0.65, and the maximum moment on the outer cylinder occurs around the dimensionless wavenumber of 0.05. Furthermore, as shown in Figure 3a, when the porosity G is increased, the dimensionless force acting on the outer cylinder decreases. This force initially increases monotonically, reaching its maximum near the dimensionless wavenumber $ka = 0.65$, before starting to decrease with increasing values of the dimensionless wavenumber ka. In the vicinity of $ka = 0.65$, the dimensionless wave force reaches its highest value, as the wave reflectivity of the outer cylinder is higher, and the dissipation also decreases. As shown in Figure 3b, the dimensionless moment attains smaller values for higher values of porosity G. It can be observed that the variations in the dimensionless moment are smaller for various values of the porosity G at low frequency. This phenomenon was also described in the study by Ning et al. [26].

In Figure 4, the dimensionless wave force $|F_{x2}/\rho g H d|$ and the dimensionless moment $\left|M_{x2}/\rho g H d^2\right|$ are plotted for a composite breakwater placed in front of an impermeable back wall against the dimensionless wavenumber ka for various values of G corresponding to $a/b = 3$, $h_1/d = 1/5$, $h_2/d = 4/5$ and $\beta = 0^\circ$. The variation in the inner cylinder moment is similar to the variation in the force of the outer cylinder. It is worth noting that the effect of variations in porosity is mostly concentrated in the lower-frequency region. From Figures 3 and 4, it can be observed that the curves are not smooth, and exhibit peaks and troughs. The strong reflection of the rigid inner wall can lead to this phenomenon. According to the derived formulas, it can be found that complex special functions (i.e., the Bessel function, the Hankel function, and their derivatives) affect the roughness of the curves.

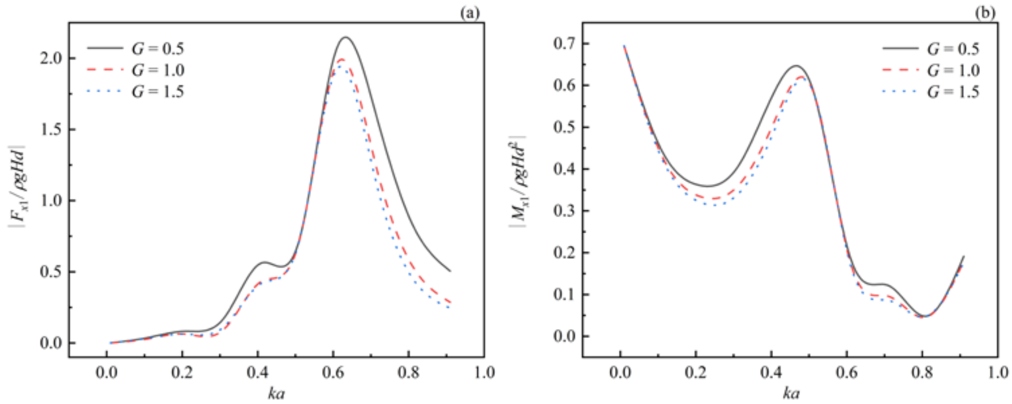

Figure 3. The magnitude of the dimensionless wave force F_{x1} and moment M_{x1} of the composite breakwater placed in front of an impermeable back wall for different values of G with $a/b = 3$, $h_1/d = 1/5$, $h_2/d = 4/5$ and $\beta = 0°$. (**a**) $|F_{x1}\ /\rho gHd|$, (**b**) $\left|M_{x1}/\rho gHd^2\right|$.

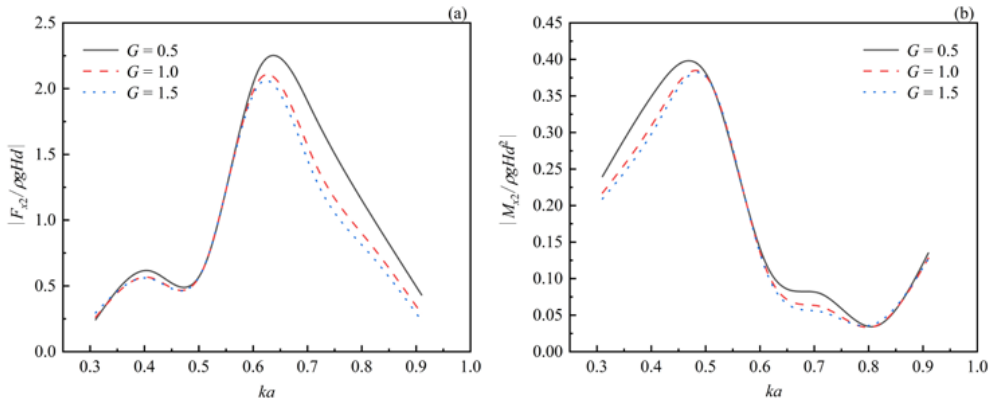

Figure 4. The magnitude of the dimensionless wave force F_{x2} and moment M_{x2} of the composite breakwater placed in front of an impermeable back wall for different values of G when $a/b = 3$, $h_1/d = 1/5$, $h_2/d = 4/5$ and $\beta = 0°$. (**a**) $|F_{x2}/|\rho gHd|$, (**b**) $\left|M_{x2}/\rho gHd^2\right|$.

Therefore, it can be concluded that the wave loads on the composite breakwater placed in front of an impermeable back wall with smaller values of porosity G are higher than those on the composite breakwater placed in front of an impermeable back wall with higher values of porosity G. Increasing porosity values G can result in a reduction in force and moment acting on the structure. However, with increasing porosity G, the safety factor and stability of the porous structure decrease. Therefore, high porosity G cannot be considered in practical engineering, and a suitable porosity G needs to be employed.

In Figure 5, the dimensionless wave force $|F_{x1}/\rho gHd|$ and the dimensionless moment $\left|M_{x1}/\rho gHd^2\right|$ are plotted for a composite breakwater placed in front of an impermeable back wall against the dimensionless wavenumber ka for various values of the ratio h_2/h_1 corresponding to $a/b = 3$, $h_1/d = 1/5$, $h_2/d = 4/5$ and $\beta = 0°$. In Figure 6, the dimensionless wave force $|F_{x2}/\rho gHd|$ and the dimensionless moment $\left|M_{x2}/\rho gHd^2\right|$ are plotted for a composite breakwater placed in front of an impermeable back wall against the dimensionless wavenumber ka for various values of the ratio h_2/h_1 corresponding to $a/b = 3$, $h_1/d = 1/5$, $h_2/d = 4/5$ and $\beta = 0°$. It can be observed that the dimensionless wave force and the dimensionless moment of the outer and inner cylinders increase when the value of the ratio h_2/h_1 increases. For the ratio $h_2/h_1 = 6$, the dimensionless wave force and the dimensionless moment distribution of the outer and inner cylinders follow the same trend as that observed when $h_2/h_1 = 4$ and 5, but are significantly higher than in the other cases because of the large area of the porous region. Increasing values of the ratio h_2/h_1 mean that the area of the porous region has also increased. It can be concluded that the larger the area of the porous region, the greater the influence the water waves will have on the cylinder. Meanwhile, the presence of an impermeable back wall allows for periodic variations in the force and moment of the structure.

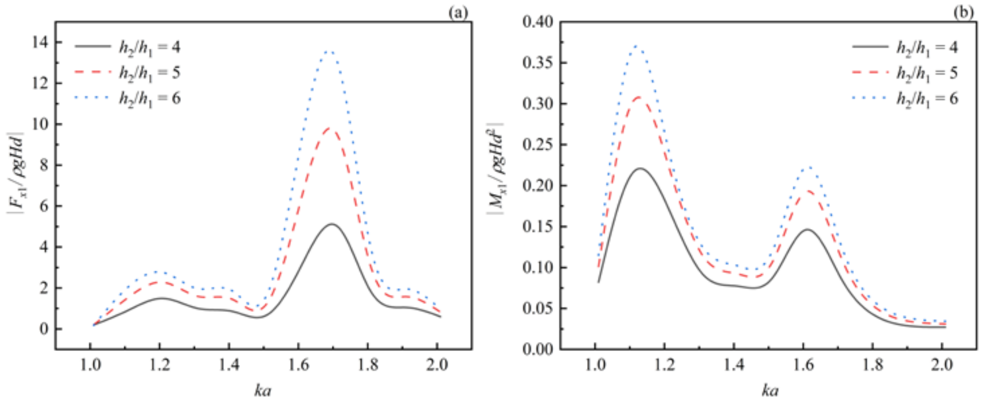

Figure 5. The magnitude of the dimensionless wave force F_{x1} and moment M_{x1} of the composite breakwater placed in front of an impermeable back wall for different values of h_1/h_2 when $a/b = 3,\ d/b = 10,\ G = 1$ and $\beta = 0°$. (**a**) $|F_{x1}/\rho gHd|$, (**b**) $|M_{x1}/\rho gHd^2|$.

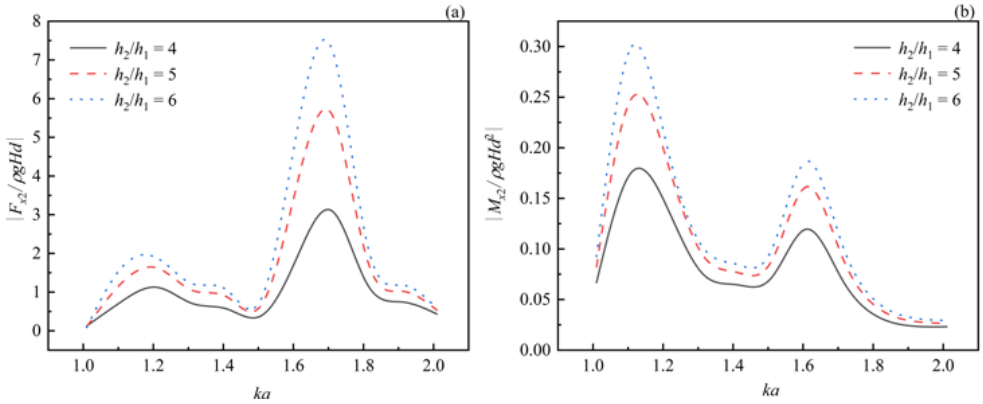

Figure 6. The magnitude of the dimensionless wave force F_{x2} and moment M_{x2} of the composite breakwater placed in front of an impermeable back wall for different values of h_2/h_1 when $a/b = 3,\ d/b = 10,\ G = 1$ and $\beta = 0°$. (**a**) $|F_{x2}/\rho gHd|$, (**b**) $|M_{x2}/\rho gHd^2|$.

Finally, it can be concluded that the dimensionless wave force and moment acting on the composite breakwater in front of the seepage-proof back wall can be reduced if an appropriate value is chosen for the ratio h_2/h_1. The composite breakwater placed in front of an impermeable back wall can be chosen properly for practical engineering, which is also beneficial for structural stability. According to the calculations in this paper, it is possible to choose a smaller value of the ratio h_2/h_1.

In Figure 7, the dimensionless wave force $|F_{x1}/\rho gHd|$ and the dimensionless moment $|M_{x1}/\rho gHd^2|$ are plotted for a composite breakwater placed in front of an impermeable back wall against the dimensionless wavenumber ka for various values of the radius ratio a/b corresponding to $h_1/d = 1/10,\ h_2/d = 4/5,\ G = 2$ and $\beta = 0°$. In Figure 8, the dimensionless wave force $|F_{x2}/\rho gHd|$ and the dimensionless moment $|M_{x2}/\rho gHd^2|$ are plotted for a composite breakwater placed in front of an impermeable back wall against the dimensionless wavenumber ka for various values of the radius ratio a/b corresponding to $h_1/d = 1/10,\ h_2/d = 4/5,\ G = 2$ and $\beta = 0°$. It can be seen that as the radius ratio a/b increases, generally speaking, the dimensionless force and the dimensionless moment on the outer and inner cylinders increase and then decrease. Some of the phenomena in this paper can be found in the same phenomena in the study by Wang and Ren [37]. Additionally, it can be observed that the dimensionless forces on the outer and inner cylinders show a cyclical variation, increasing and then decreasing with increasing values of the dimensionless wavenumber. The reason for this is the occurrence of constructive interference between the incident and reflected waves. Furthermore, when the dimensionless wavenumber $ka > 1$, the dimensionless force and the dimensionless moment on the outer and inner cylinders change pronouncedly when the radius ratio is set to $a/b = 5$. Three values of radius ratio are considered in this paper, and from the results of the calculations, the radius ratio of $a/b = 4$ was found to be the most suitable for effective control of wave loads. Therefore, it can be concluded that choosing the right radius ratio a/b reduces the degree to which wave forces act on the inner and outer cylinders. It is clear from the calculations in this paper that, in addition to choosing a suitable radius ratio a/b, a smaller wavenumber can also be chosen to reduce the force and moment acting on the structure.

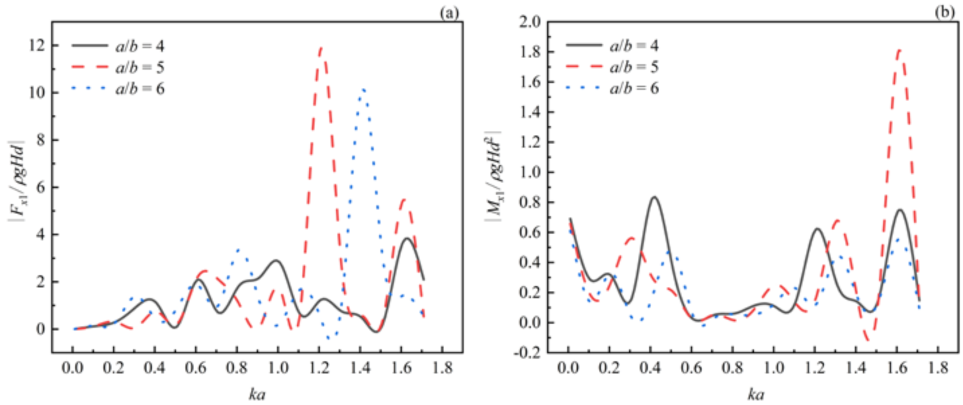

Figure 7. The magnitude of the dimensionless wave force F_{x1} and moment M_{x1} of the composite breakwater placed in front of an impermeable back wall for different values of a/b when $h_1/d = 1/10$, $h_2/d = 4/5$, $G = 2$ and $\beta = 0°$. (**a**) $|F_{x1}/\rho gHd|$, (**b**) $\left|M_{x1}/\rho gHd^2\right|$.

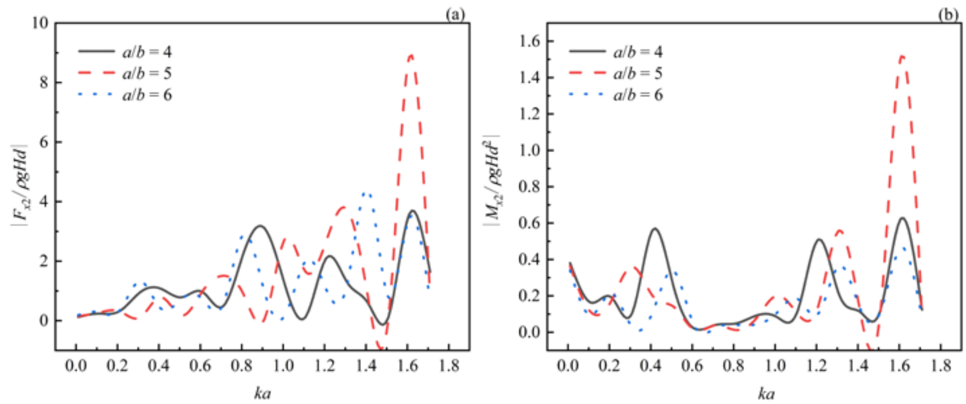

Figure 8. The magnitude of the dimensionless wave force F_{x2} and moment M_{x2} of the composite breakwater placed in front of an impermeable back wall for different values of a/b when $h_1/d = 1/10$, $h_2/d = 4/5$, $G = 2$ and $\beta = 0°$. (**a**) $|F_{x2}/\rho gHd|$, (**b**) $\left|M_{x2}/\rho gHd^2\right|$.

The amplitudes of the waves on the surface of the composite breakwater placed in front of an impermeable back wall—the dimensionless wave amplitudes $|\eta_1/A|$ and $|\eta_2/A|$—are shown in Figure 9 as polar plots. The calculated parameters are $a/b = 2, h_1/d = 1/10$, $G = 3$ and $h_2/d = 9/10$. $|\eta_1/A|$ and $|\eta_2/A|$ denote the amplitude of the dimensionless wave on the outer cylinder and the inner cylinder, respectively. The dimensionless wave amplitude at the free surface is considered for five different dimensionless wavenumber values: ka= 0.1, 0.2, 0.3,0.4 and 0.5. It can be seen that the change in the dimensionless wavenumber has a greater effect on the outer cylinder and a smaller effect on the inner cylinder at higher frequencies, with the wave creep being more significant at high frequencies. This is because the impermeable back wall affects the outer cylinder more than the inner cylinder. The presence of the impermeable back wall causes the wave amplitude on the outer cylinder to vary significantly with wavenumber.

Therefore, in practical engineering, the study of structures placed in front of an impermeable back wall can be undertaken by choosing a smaller wavenumber, thus reducing the wave amplitude acting on the cylinder.

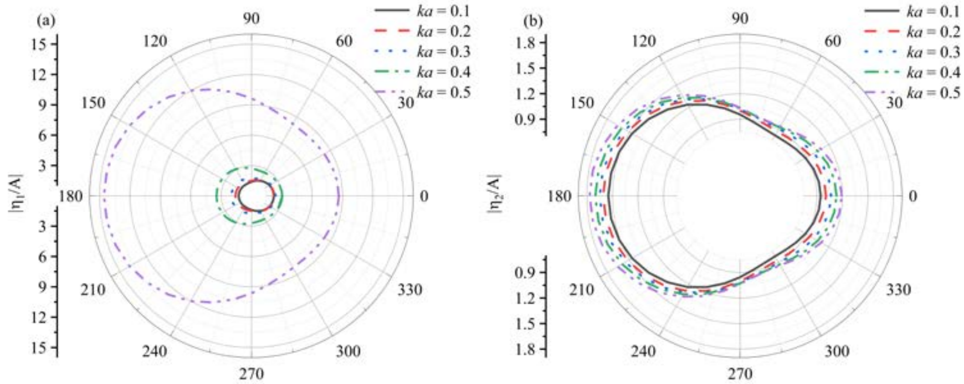

Figure 9. The dimensionless wave amplitude $|\eta_1/A|$ and $|\eta_2/A|$ at the free surface when $a/b = 2, h_1/d = 1/10, h_2/d = 9/10$ and $G = 3$. (**a**) the amplitude of the dimensionless wave on the outer cylinder, (**b**) the amplitude of the dimensionless wave on the inner cylinder.

4.2.2. A Composite Breakwater

In order to understand the influence of these parameters on the composite breakwater, a study is carried out on the outer cylinder of the composite breakwater, focusing on the variation in the outer cylinder. In Figure 10, the dimensionless wave force $|f_{x1}/\rho g H \pi a^2|$ for the outer cylinder is plotted against the dimensionless wavenumber ka for various values of G corresponding to $a/b = 3$, $h_1/d = 1/5$, $h_2/d = 4/5$ and $\beta = 0°$. The dimensionless wave force acting in Figure 10 is similar to the dimensionless wave force presented in Figures 3a and 4a. As shown in Figure 10, lower values are attained for the dimensionless wave force with higher values of porosity G. It can be seen that the maximum force on the outer cylinder occurs around the dimensionless wavenumber of 0.7. Therefore, it can be concluded that the wave loads on the composite breakwater with lower values of porosity G are higher than those on the composite breakwater with higher values of porosity G.

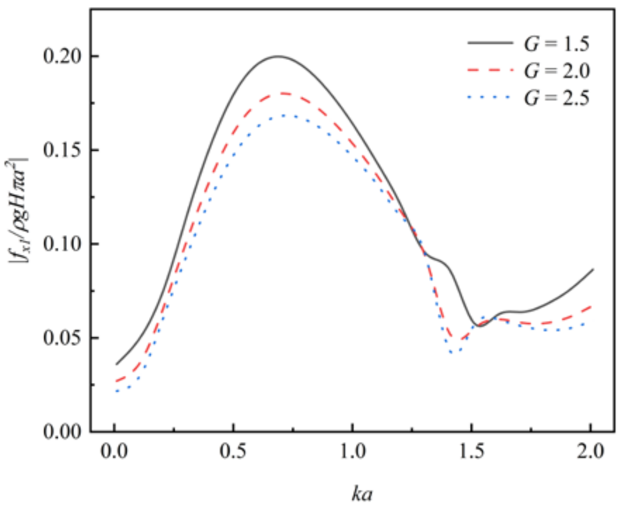

Figure 10. The magnitude of the dimensionless wave force f_{x1} of the composite breakwater for different values of G with $a/b = 3$, $h_1/d = 1/5$, $h_2/d = 4/5$ and $\beta = 0°$.

In Figure 11, the dimensionless wave force $|f_{x1}/\rho g H \pi a^2|$ for the outer cylinder is plotted against the dimensionless wavenumber for various values of the ratio h_2/h_1 corresponding to $a/b = 3$, $d/b = 10$, $G = 1$ and $\beta = 0°$. When the dimensionless wavenumber $1.6 \leq ka \leq 2.0$, the dimensionless wave force acting in Figure 11 is similar to the dimensionless wave force presented in Figures 5a and 6a, and when the dimensionless wavenumber $1.0 \le ka \le 1.6$, the dimensionless wave force acting in Figure 11 is not the same as the dimensionless wave force presented in Figures 5a and 6a, because the impermeable back wall has a greater impact on the composite breakwater at low frequencies.

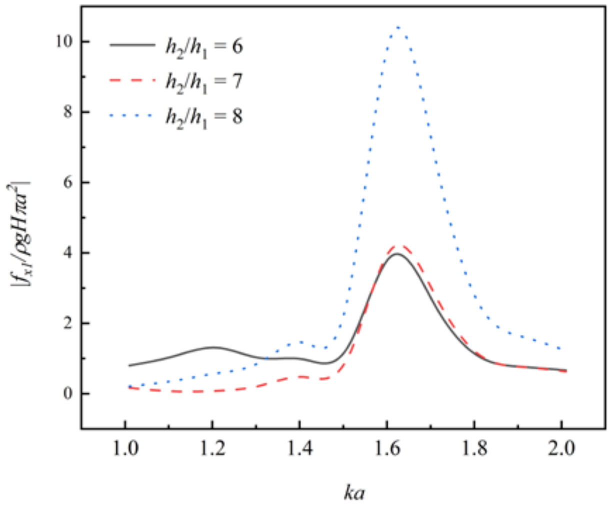

Figure 11. The magnitude of the dimensionless wave force f_{x1} of the composite breakwater for different values of h_2/h_1 with $a/b = 3$, $d/b = 10$, $G = 1$ and $\beta = 0°$.

In Figure 12, the dimensionless wave force $|f_{x1}/\rho gH\pi a^2|$ for the outer cylinder is plotted against the dimensionless wavenumber for various values a/b corresponding to $h_1/d = 1/10$, $h_2/d = 4/5$, $G = 2$ and $\beta = 0°$. The dimensionless wave force acting in Figure 12 is not the same as the dimensionless wave force presented in Figures 7a and 8a. Because there is no impermeable back wall, the dimensionless wave force acting on the outer cylinder shows a certain pattern as the radius ratio a/b changes. When $a/b = 4$, the distribution of dimensionless wave force and the dimensionless moment in the outer cylinder follows the same trend as when a/b= 5 and 6. It can be observed that all curves of the dimensionless wave force on the outer cylinder initially increase, and then decrease with increasing dimensionless wavenumber values. This shows a cyclical pattern. From this, it can be found that the dimensionless wave force on the outer cylinder can be reduced by an appropriate radius ratio a/b. The dimensionless wave loads can be effectively controlled by choosing the appropriate radius ratio a/b of the composite breakwater.

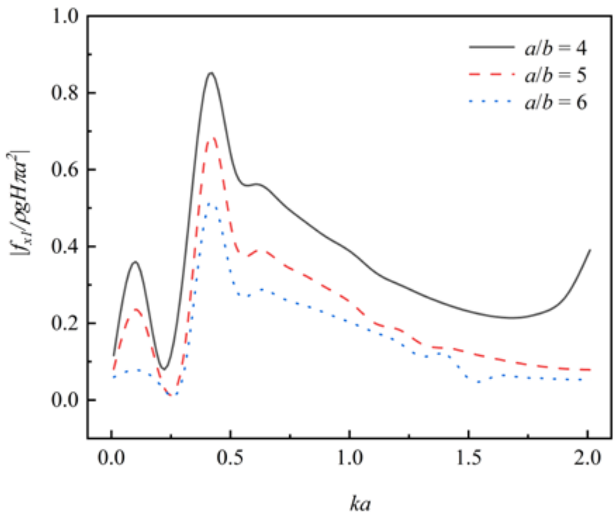

Figure 12. The magnitude of the dimensionless wave force f_{x1} of the composite breakwater for different values of a/b when $h_1/d = 1/10$, $h_2/d = 4/5$, $G = 2$ and $\beta = 0°$.

Special attention needs to be paid to the fact that, for coaxial structures, the oscillation of water waves inside the system space can slowly destroy the structure. Therefore, a suitable radius ratio needs to be considered for safety purposes in practical engineering.

The amplitudes of the wave on the surface of the composite breakwater—the dimensionless wave amplitudes $|\zeta/A|$—are shown in Figure 13 as polar plots for $a/b = 2$, $h_1/d = 1/10$, $h_2/d = 9/10$ and $G = 3$. $|\zeta/A|$ denotes the dimensionless wave amplitude on the outer cylinder. The dimensionless wave amplitude at the free surface is considered for three different dimensionless wavenumber values. In Figure 13, it can be seen that when the wavenumber is small, the change in wave run-up is not obvious, and when the dimensionless wavenumber becomes larger, the wave run-up increases more significantly. Additionally, as the angle increases, the dimensionless wave run-up becomes larger. This is due to the interaction of the incident and scattered waves causing a change near the cylinder.

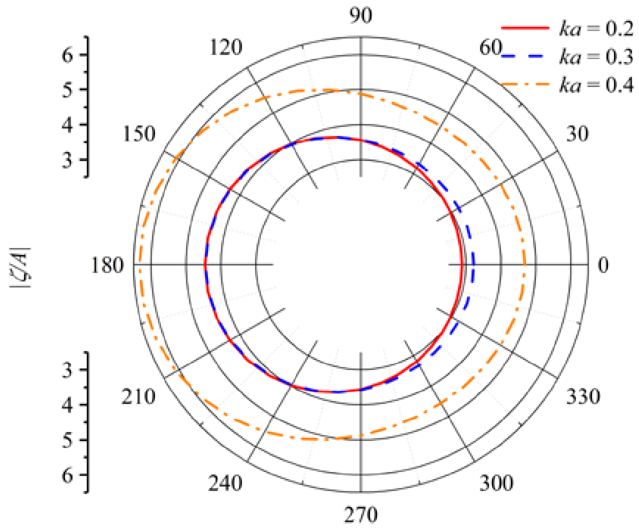

Figure 13. The dimensionless wave amplitude $|\zeta/A|$ at the free surface for $a/b = 2$, $h_1/d = 1/10$, $h_2/d = 9/10$ and $G = 3$.

5. Conclusions

The current work presented a theoretically study of the interaction of linear water waves with a composite breakwater placed in front of an impermeable back wall. Additionally, to fully understand composite breakwaters, the same method was used to develop a composite breakwater. In this paper, the problem of Laplace equation control was solved by using the eigenfunction expansion approach and the separation of variables technique. The complete mathematical formulation was given based on the potential flow theory using the eigenfunction expansion method and Darcy's law. The conclusions are as follows:

1. The dimensionless wave force and the dimensionless moment acting on the outer and inner cylinders decrease when the porosity G increases. Although increasing the porosity can reduce the force and moment acting on the structure, too much porosity can have an impact on the safety and stability of the structure. Therefore, the porosity needs to be chosen to have the minimum impact on the outer and inner cylinders.
2. The dimensionless wave force acting on the outer and inner cylinders is smaller in the case of short waves, and vice versa. Additionally, the selection of larger h_2/h_1 can minimize the dimensionless wave force on the composite breakwater to be beneficial for structural stability. However, for a composite breakwater placed in front of an impermeable back wall, because of the presence of the impermeable back wall, it is necessary to select a smaller ratio h_2/h_1.
3. With the coaxial structure, the oscillation of water waves inside the system space can slowly destroy the structure. Choosing the right radius ratio a/b reduces the wave

forces acting on the inner and outer cylinders, and the wave loads can be effectively controlled.

Finally, the reflection coefficient of the upright wall was not calculated in this paper, and will be investigated in detail in future studies. Considering the actual situation of the present study, it is believed that additional research could be performed to better understand the stability of a composite breakwater when placed in front of an impermeable back wall. Future investigations considering the role of bottom undulation in the interaction of waves with a composite breakwater placed in front of an impermeable back wall in the presence of a porous seabed could be of significant interest.

Author Contributions: Conceptualization, J.C.; methodology, J.C. and Z.W.; software, J.C. and Z.W.; validation, C.W.; investigation, C.W.; writing—original draft preparation, J.C.; writing—review and editing, J.C., C.W. and Z.W.; supervision, Z.W.; funding acquisition, J.C. and C.W. All authors have read and agreed to the published version of the manuscript.

Funding: This research was funded by the National Natural Science Foundation of China, Fund No. 51679052, 51809055, 51909043 and the PhD Student Research and Innovation Fund of the Fundamental Research Funds.

Institutional Review Board Statement: Not applicable.

Informed Consent Statement: Not applicable.

Data Availability Statement: Data are only available on request due to restrictions, e.g., privacy or ethical. The data presented in this study are available on request from the corresponding author.

Conflicts of Interest: The authors declare no conflict of interest.

References

1. Liu, Y.; Li, Y.-c.; Teng, B. Wave interaction with a perforated wall breakwater with a submerged horizontal porous plate. *Ocean Eng.* **2007**, *34*, 2364–2373. [CrossRef]
2. Athul Krishna, K.R.; Abdulla, K.; Karmakar, D. Dissipation of gravity waves due to submerged porous plate coupled with porous structures. *J. Offshore Mech. Arct. Eng.* **2022**, *145*, 011201. [CrossRef]
3. Lee, J.-I.; Shin, S. Experimental study on the wave reflection of partially perforated wall caissons with single and double chambers. *Ocean Eng.* **2014**, *91*, 1–10. [CrossRef]
4. Zhao, Y.; Liu, Y.; Li, H. Iterative analytical solution for wave reflection by a multi-chamber partially perforated caisson breakwater. *Acta Oceanol. Sin.* **2020**, *39*, 115–126. [CrossRef]
5. Li, Y.; Liu, H.-j.; Dong, G.-h. The force of oblique incident wave on the breakwater with a partially perforated wall. *Acta Oceanol. Sin.* **2005**, *24*, 121–130.
6. Suh, K.-D.; Park, J.K.; Park, W.S. Wave reflection from partially perforated-wall caisson breakwater. *Ocean Eng.* **2006**, *33*, 264–280. [CrossRef]
7. Jarlan, G.E. A perforated vertical wall breakwater. *Dock Harb. Auth. XII* **1961**, *486*, 394–398.
8. Jarlan, A.-G.E. The application of acoustic theory to the reflective properties of coastal engineering structures. *Bull. Natl. Res. Counc. Can.* **1965**, *1*, 23–64.
9. Isaacson, M.; Baldwin, J.; Allyn, N.; Cowdell, S. Wave Interactions with Perforated Breakwater. *J. Waterw. Port Coast. Ocean. Eng.* **2000**, *126*, 229–235. [CrossRef]
10. Garrido, J.M.; Medina, J.R. New neural network-derived empirical formulas for estimating wave reflection on Jarlan-type breakwaters. *Coast. Eng.* **2012**, *62*, 9–18. [CrossRef]
11. Yang, H.T.O.; Huang, L.H.; Hwang, W.S. The interference of a semi-submerged obstacle on the porous breakwater. *Appl. Ocean Res.* **1997**, *19*, 263–273. [CrossRef]
12. Williams, A.N.; Mansour, A.-E.M.; Lee, H.S. Simplified analytical solutions for wave interaction with absorbing-type caisson breakwaters. *Ocean Eng.* **2000**, *27*, 1231–1248. [CrossRef]
13. Li, Y.; Dong, G.; Liu, H.; Sun, D. The reflection of oblique incident waves by breakwaters with double-layered perforated wall. *Coast. Eng.* **2003**, *50*, 47–60. [CrossRef]
14. Liu, Y.; Li, Y.-c. Wave interaction with a wave absorbing double curtain-wall breakwater. *Ocean Eng.* **2011**, *38*, 1237–1245. [CrossRef]
15. Liu, Y.; Li, Y.-C.; Teng, B. Interaction between obliquely incident waves and an infinite array of multi-chamber perforated caissons. *J. Eng. Math.* **2012**, *74*, 1–18. [CrossRef]
16. Liu, Y.; Li, Y.-c.; Teng, B. Interaction between oblique waves and perforated caisson breakwaters with perforated partition walls. *Eur. J. Mech.-B/Fluids* **2016**, *56*, 143–155. [CrossRef]

17. Mohapatra, A.K.; Sahoo, T. Surface Gravity Wave Interaction With a Submerged Composite Wavy Porous Plate Attached to a Vertical Wall. *J. Offshore Mech. Arct. Eng.* **2021**, *144*, 011904. [CrossRef]
18. Behera, H.; Sahoo, T. Gravity wave interaction with porous structures in two-layer fluid. *J. Eng. Math.* **2013**, *87*, 73–97. [CrossRef]
19. Chang, J.-Y.; Tsai, C.-C. Wave Forces on a Partially Reflecting Wall by Oblique Bragg Scattering with Porous Breakwaters over Uneven Bottoms. *J. Mar. Sci. Eng.* **2022**, *10*, 409. [CrossRef]
20. Tsai, C.-C.; Behera, H.; Hsu, T.-W. Analysis of water wave interaction with multiple submerged semi-circular porous structures. *Arch. Appl. Mech.* **2023**, *93*, 2693–2709. [CrossRef]
21. Zhai, Z.; Zheng, S.; Wan, D. Interaction between solitary waves and a combined structure of two concentric asymmetric porous arc walls. *Phys. Fluids* **2022**, *34*, 042103. [CrossRef]
22. Zhai, Z.; Li, H.; Zhang, A.; An, S.; Wang, K. Analytical modelling of water wave diffraction by a bottom-mounted surface-piercing concentric dual-arc porous thin wall. *Ocean. Eng.* **2021**, *236*, 109485. [CrossRef]
23. Williams, A.N.; Li, W. Wave interaction with a semi-porous cylindrical breakwater mounted on a storage tank. *Ocean Eng.* **1998**, *25*, 195–219. [CrossRef]
24. Sankarbabu, K.; Sannasiraj, S.A.; Sundar, V. Interaction of regular waves with a group of dual porous circular cylinders. *Appl. Ocean Res.* **2007**, *29*, 180–190. [CrossRef]
25. Liu, J.; Lin, G.; Li, J. Short-crested waves interaction with a concentric cylindrical structure with double-layered perforated walls. *Ocean Eng.* **2012**, *40*, 76–90. [CrossRef]
26. Ning, D.-Z.; Zhao, X.-L.; Teng, B.; Johanning, L. Wave diffraction from a truncated cylinder with an upper porous sidewall and an inner column. *Ocean. Eng.* **2017**, *130*, 471–481. [CrossRef]
27. Park, M.-S.; Jeong, Y.-J. Water Wave Interaction by Dual Cylindrical Caisson Breakwater with Partial Porous Area. In *ASIAN AND PACIFIC COASTS 2017: Proceedings of the 9th International Conference on Asia and Pacific Coasts 2017 (APAC 2017), Pasay City, Philippines, 19–21 October 2017*; World Scientific Publishing Co Pte Ltd.: Singapore, 2017; pp. 695–704.
28. Liu, J.; Guo, A.; Nandasena, N.A.K.; Melville, B.W.; Li, H. Theoretical and experimental investigation on wave interaction with a concentric porous cylinder form of breakwater. *Ocean Eng.* **2018**, *160*, 156–167. [CrossRef]
29. Sarkar, A.; Bora, S.N. Hydrodynamic force and wave run-up due to diffraction of ocean water waves by a surface-piercing bottom-mounted compound partial-porous cylinder. *Fluid Dyn. Res.* **2021**, *53*, 015508. [CrossRef]
30. Williams, A.N.; Li, W.; Wang, K.H. Water wave interaction with a floating porous cylinder. *Ocean Eng.* **2000**, *27*, 1–28. [CrossRef]
31. Dalrymple, R.A.; Losada, M.A.; Martin, P.A. Reflection and transmission from porous structures under oblique wave attack. *J. Fluid Mech.* **1991**, *224*, 625–644. [CrossRef]
32. Barman, K.K.; Bora, S.N. Scattering and trapping of water waves by a composite breakwater placed on an elevated bottom in a two-layer fluid flowing over a porous sea-bed. *Appl. Ocean. Res.* **2021**, *113*, 102544. [CrossRef]
33. Losada, I.J.; Silva, R.; Losada, M.A. 3-D non-breaking regular wave interaction with submerged breakwaters. *Coast. Eng.* **1996**, *28*, 229–248. [CrossRef]
34. Wu, J.; Wan, Z.; Fang, Y. Wave reflection by a vertical wall with a horizontal submerged porous plate. *Ocean Eng.* **1998**, *25*, 767–779. [CrossRef]
35. MacCamy, R.C.; Fuchs, R.A. *Wave Forces on Piles: A Diffraction Theory*; U.S. Beach Erosion Board: Vicksburg, MS, USA, 1954.
36. Mackay, E.; Shi, W.; Qiao, D.; Gabl, R.; Davey, T.; Ning, D.; Johanning, L. Numerical and experimental modelling of wave interaction with fixed and floating porous cylinders. *Ocean Eng.* **2021**, *242*, 110118. [CrossRef]
37. Wang, K.-H.; Ren, X. Wave interaction with a concentric porous cylinder system. *Ocean Eng.* **1994**, *21*, 343–360. [CrossRef]